Instituto de Física
Universidade de São Paulo

Simulation of coherent X-ray radiation produced by relativistic charged particles in crystals

V.B. Gavrikov[1)], V.P. Likhachev[2)], J.D.T. Arruda-Neto[2,3)], A. Deppman[2)], A.L. Bonini[2)]

[1)] Kharkov Institute of Physics and Technology, 1 Akademishna, 61108, Kharkov, Ukraine

[2)] Experimental Physics Department, Physics Institute, University of Sao Paulo, SP, Brazil

[3)] University of Santo Amaro /UNISA, Sao Paulo, Brazil

Publicação IF - 1559/2003

Simulation of coherent X-ray radiation produced by relativistic charged particles in crystals

V.B. Gavrikov[1], V.P. Likhachev[2], J.D.T. Arruda-Neto[2,3], A.L. Bonini[2]

[1] *Kharkov Institute of Physics and Technology,*

1 Akademishna 61108

Kharkov, Ukraine

[2] *Instituto de Física da Universidade de São Paulo,*

CP66318, 05315-970 São Paulo, SP, Brazil

[3] *University of Santo Amaro/UNISA, Brazil*

(Dated: January 21, 2003)

Abstract

We developed a Monte Carlo (MC) code to simulate coherent X-ray radiation (CXR), produced by relativistic charged particles in diamond-like crystals. The code calculates both the number of coherent photons under CXR peaks, as a function of the crystal target orientation with respect to the beam direction, and the shape of a CXR line at fixed crystal orientation. The calculations are carried out in the Laue geometry and for observation angles $\theta > \gamma^{-1}$, where γ is the projectile Lorentz factor. The MC simulation takes into account multiple scattering process, attenuation of the photon flux in the target and detector window, finite detector acceptance and energy resolution of a detector. The developed code can be used to study the potentialities of CXR applications and to the planing of further experiments with CXR.

I. PROGRAM SUMMARY

Title of program: CXR

Catalogue number:

Program obtainable from:

Computer for which the program was designed and others on which it is operable: Microcomputer with Intel 80386+80387, Intel 80486+80487, and Pentium Intel 233.

Installations: Physics Institute, University of Sao de Paulo, Sao Paulo, Brazil.

Operating systems under which the program has been tested: MS-DOS 6.00, Windows 95/98 and Windows NT 3.5.

Programming language used: Turbo Pascal 7.0

Memory required to execute with typical data: 8 Mbytes of RAM memory and 1 Mb of hard disc memory.

No. of bits in a word: 16

No. of bytes in distributed program, including test data, etc.: 405031

Distribution format: ASCII files, CXR.EXE

Keywords: coherent X-radiation, coherent bremsstrahlung, parametric X-radiation, Monte Carlo method

II. *NATURE OF PHYSICAL PROBLEM*

The interaction of a relativistic charged particle with a crystalline medium leads to the appearance of a row of physical effects due to the ordered character of such medium and do not show up themselves in amorphous mediums. One of these effects is coherent X-ray radiation (CXR). This radiation arises because in crystals, and in the X-ray energy range, radiation probabilities have sharp maxima at those momenta transferred to the medium which are very close to the reciprocal lattice vectors. The first experimental observation of CXR was performed at Tomsk (Russia) synchrotron "Siriys" in 1985, [1]. Due to difficulties in measuring a charge passing through a target during exposition to radiation spectra, the authors of this work came to the conclusion that the radiation observed by them is Cherenkov radiation in the X-ray energy region. Later, much finer experimental methods and equipment have been developed, allowing the elucidation of the question about the nature of CXR. It

were carried out absolute measurements of radiation intensity in silicon, germanium and diamond crystals, by using linear accelerators with electron beam energies of tens of MeV. In particular, the integral number of photons under the CXR peak, as a function of the crystal orientation, were measured in silicon crystal at 15, 15.75 and 25 MeV ([2],[3]), in germanium crystal at 21.6 and 25.4 MeV ([3],[4]), and in diamond crystal at beam energies below 10 MeV [5]. The first information concerning observation of the interference effect between polarization and static bremsstrahlung mechanisms of the radiation was provided by the authors of Ref. [6] and the analysis of these results was made in Refs. [7] and [8]. Shape and orientation dependence of CXR linewidths were for the first time experimentally and numerically investigated by Adejishvili *et al.* [9] using a Monte-Carlo simulation for a germanium crystal at electron beam energy of 25.4 MeV. Note that the above mentioned works stimulated a large number of other experiments where the CXR properties where investigated, and the results of these seminal works have been confirmed. The years of investigations on CXR are summarized in Refs. [10] and [11], where analytical expressions describing CXR intensity and shape of the radiation line were obtained in the small-angle multiple scattering approximation. It was quantitatively shown advantages as high energy resolution, easy tunable energy, high degree of linear polarization, as well as disadvantages like low intensity of CXR.

It is nowaday a needed aim to find fields for application of CXR, which effectively use the advantages of CXR and do not need the high intensity.

To estimate the potentiality of CXR for particular applications, and to plan further experiments where CXR would be used, one need to calculate the radiation characteristics at arbitrary sets of working parameters. The more natural way for calculations is a Monte Carlo procedure, and the present work is devoted to the description of such a code. The algorithms are based on the theoretical approaches described in Refs [12], [14], [13]. The code was already used for studies of CXR characteristics in Refs [15], [16], [8], [11].

III. *METHOD OF SOLUTION*

The Monte Carlo simulation, which takes multiple scattering process, attenuation of the photon flux in the target and detector window, finite detector acceptance and energy resolution of a detector into account.

Restrictions on the complexity of the problem

The CXR code makes calculations for crystals with diamond-like structure, i.e., for diamond, silicon and germanium crystals, and it is assumed that the radiation is generated in the Laue geometry, i.e., coherent photons and relativistic particles exit on the same side of the crystal, and channeling radiation does not occur. Moreover, we assume that: (1) the momentum of the projectile is much larger than momenta of radiated photons and, therefore, the influence of the radiation on the projectile motion can be neglected; (2) the thickness of a target is such that energy loses of the projectile can be neglected; (3) polarization states of bremsstrahlung photons are not observed; (4) detector angular size is much less than γ^{-1} and (5) the trajectory of the projectile inside the crystal is approximated by straight lines.

Typical running time: Depends on the choice for calculations. For a particular set of parameters the running time is approximately 120 seconds.

IV. LONG WRITE-UP

A. CXR Cross section

Quantum theory of bremsstrahlung, arising due to interaction of a relativistic charged particle with an atom as a whole, was developed by Amusia *et. al.* ([13], [17]) and, a crystal case, was considered by Nitta ([18]).

The nature of coherent X-radiation can be explained as a result of constructive interference of the bremsstrahlung emitted by a relativistic charged particle, passing through a crystal, and bremsstrahlung resulting from bound atomic electrons in the crystal. The three-order Feynman diagrams describing the radiation amplitudes are presented in Fig. 1.

In the X-ray energy range the crystal band structure can be neglected, and the radiation cross section per an atom in a crystal can be expressed through a cross section for an isolated atom $d\sigma_{at}$ and the diffraction factor, as it was performed in the theory of high-energy coherent bremsstrahlung ([19],[20]). Therefore, we can consider firstly the atomic cross section which can be written in the ordinary form

$$d^6\sigma_{at} = 2\pi \left| M_{at}\left(\overrightarrow{p}_{i,f}; \overrightarrow{k}; \overrightarrow{e}_f; \overrightarrow{q}\right)\right|^2 \delta\left(E_i - E_f - \omega\right) \frac{d^3p_f d^3k}{\left(2\pi\right)^6}, \qquad (1)$$

where $\overrightarrow{p}_i, E_i$ and $\overrightarrow{p}_f, E_f$ are the initial and final momenta and energies of the projectile,

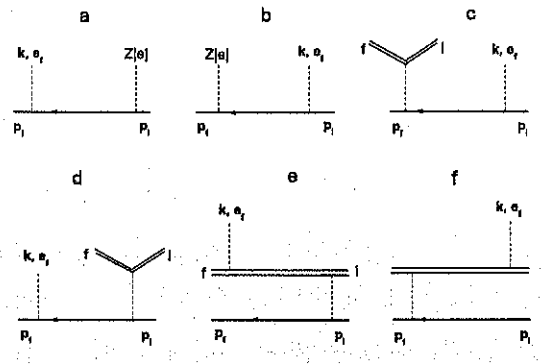

FIG. 1: The third-order perturbative theory diagrams. The solid lines, the twin-solid lines and the dashed lines represent the relativistic charged particle, crystal electrons and bremsstrahlung photon, respectively. *a*, *b*, *c* and *d* diagrams show bremsstrahlung processes (BS); *e* and *f* diagrams represent polarization bremsstrahlung processes (PR).

respectively; $\overrightarrow{k}, \overrightarrow{e}_f, \omega$ are the momentum, vector of polarization and energy of a radiated photon; $\overrightarrow{q} = \overrightarrow{p}_i - \overrightarrow{p}_f - \overrightarrow{k}$ is the recoil momentum.

By assuming that: (1) the atom does not change its state during the interaction; (2) the inequality $\omega << E_i, E_f$ is satisfied for all relevant photon energies and (3) the radiation energies are large compared to the electronic binding ones, the full amplitude of the radiation process for a nonrelativistic atom has the form ([13], [17]):

$$|M_{at}|^2 = \left|M^{BS} + M^{PR}\right|^2 = \frac{2^5\pi^3}{\omega}\left|\overrightarrow{e_f}\left\{-\frac{ee_0^2}{m_0\gamma q^2}\left(Z - F\left(\overrightarrow{q}\right)\right)\frac{\overrightarrow{q}}{\omega - \overrightarrow{k}\,\overrightarrow{v}} + \frac{e^2e_0}{m}\frac{F\left(\overrightarrow{q}\right)}{\omega}\frac{\overrightarrow{v}\omega - \overrightarrow{q}}{\left(\overrightarrow{q} + \overrightarrow{k}\right)^2 - \omega}\right.\right. \quad (2)$$

In Eq.(2) $\overrightarrow{v}$ is the particle velocity; γ is the projectile Lorentz factor; e_0 and m_0 are the charge and mass of the relativistic particle; e and m are the charge and mass of the electron ; $F\left(\overrightarrow{q}\right)$ is the atomic form factor; Z is the atomic number. M^{BS} describes the relativistic bremsstrahlung of the particle (diagrams *a*, *b*, *c* and *d* in Fig.1) and M^{PR} results from polarisation bremsstrahlung of the atomic electrons (diagrams *e* and *f* in Fig.1).

It was shown in Ref. [19] that the perturbative theory can be applied not only to an atom but to a crystal too. The proposed method was successfully applied in calculating the cross section of high-energy bremsstrahlung and electron pair production in thin crystals ([19],

[20]). Every atom of a crystal gives the radiation amplitude $M_{at}\exp\left(-i\vec{q}\,\vec{R}_{\vec{L}}\right)$, where $\vec{R}_{\vec{L}}$ are the relative coordinates of crystal atoms and, therefore, in the crystal medium the total cross section of the process, described by the diagrams in Fig. 1, differs from Eq.(1) by the diffraction factor $\left|\sum\limits_{\vec{L}}\exp\left(-i\vec{q}\,\vec{R}_{\vec{L}}\right)\right|^2$.

For an actual crystal the diffraction factor, normalised to one crystal cell and averaged over thermal vibrations, has the form

$$\left\langle\left|\sum_{\vec{L}}\exp\left(-i\vec{q}\,\vec{R}_{\vec{L}}\right)\right|^2\right\rangle_{\vec{u}} = D\left(\vec{q}\right)S^2\left(\vec{q}\right)\exp\left(-q^2u^2\right)+N\left[1-\exp\left(-q^2u^2\right)\right], \quad (3)$$

where N is the number of atoms per unit cell; $S^2\left(\vec{q}\right)$ is the crystal structure factor; $\exp\left(-q^2u^2\right)$ is the Debye-Waller factor; u^2 is a mean-square temperature displacement of the crystal atoms from their equilibrium positions; $D\left(\vec{q}\right)$ is the diffraction factor of the ideal crystal with N_1 periods in the direction of crystal thickness and with large numbers of periods, $N_2, N_3 \to \infty$, in the crosswise directions:

$$D\left(\vec{q}\right) = \lim_{N_2,N_3\to\infty}\left[\prod_{j=1}^{3}\frac{\sin^2\left(\frac{N_j}{2}\vec{q}\,\vec{a}_j\right)}{N_j\sin^2\left(\frac{1}{2}\vec{q}\,\vec{a}_j\right)}\right] = \frac{(2\pi)^2 a_1}{V}\sum_{\vec{g}}\delta\left(\vec{q}-\vec{g}\right)_{\perp\vec{n}}\frac{\sin^2\left(\frac{N_1}{2}\vec{q}\,\vec{a}_1\right)}{N_1\sin^2\left(\frac{1}{2}\vec{q}\,\vec{a}_1\right)}, \quad (4)$$

where $\vec{a}_j\,(j=1,2,3)$ are the lattice basis vectors; $V = a_1a_2a_3$ is the volume of the unit crystal cell; $\vec{g}$ are a set of crystal reciprocal lattice vectors; $\vec{n} = \vec{a}_1/a_1$ is the unit vector in the direction of the crystal thickness. In Eq.(4) the symbol $\perp\vec{n}$ means than the δ-function argument is a vector component, which is perpendicular to $\vec{n}$.

As it follows from Eq.(3), the total (BS plus PR) bremsstrahlung in a crystal subdivides into two terms. The first one is a coherent term; it is proportional to $\exp\left(-q^2u^2\right)$ and it gives a contribution to the interference effects. The second term is an incoherent one; it is due to the thermal vibrations of the crystal atoms.

To obtain the CXR cross section we have to multiply Eq.(1) on the first part of the diffraction factor, Eq.(3), and then integrate the coherent cross section over d^3p_f. Introducing new variables $\vec{p}_i - \vec{p}_f = \vec{p}_1, E_i - E_f = E_1$, and using equality $\vec{p}_1\vec{v} = E_1$, we can replace $\delta\left(\vec{q}-\vec{g}\right)_{\perp\vec{n}}\delta\left(E_i-E_f-\omega\right)d^3p_f$ by $\delta\left(\vec{p}_1-\vec{k}-\vec{g}\right)_{\perp\vec{n}}\delta\left(E_1-\omega\right)\left(\vec{v}\,\vec{n}\right)^{-1}d^2p_{1,\perp\vec{n}}dE_1$. After integrating, and by using the

limit transition $N_1 \to \infty$, we obtain the following expression for the CXR spectral-angular cross section

$$\left(\frac{d^3\sigma}{d\omega d\Omega}\right)_{coh} = \frac{8\pi\omega}{V\left(1-\vec{v}\,\vec{n}_k\right)} \sum_{\vec{g},f} \left|M_{cr}\right|^2 S^2\left(\vec{g}\right) \exp\left(-g^2u^2\right) \delta\left(\omega - \frac{\vec{g}\,\vec{v}}{1-\vec{v}\,\vec{n}_k}\right), \qquad (5)$$

where $\vec{n}_k = \vec{k}/k$, and the summation in Eq.(5) is over all reciprocal lattice vectors $\vec{g}$ and photon polarization directions. In Eq.(5) the matrix element has the form

$$\left|M_{cr}\right|^2 = \left|M^{BS} + M^{PR}\right|^2 = \frac{e^6}{\omega^2 m^2} \left| \vec{e_f} \left\{ -\frac{e_0 m}{e m_0 \gamma g^2} \left(Z - F\left(\vec{q}\right)\right) \frac{\vec{g}}{1-\vec{v}\,\vec{n}_k} + F\left(\vec{g}\right) \frac{\vec{v}\omega - \vec{g}}{\left(\vec{q}+\vec{k}\right)^2 - k^2} \right\} \right. \qquad (6)$$

The energy of the radiated photon is defined by equating the δ-function argument in Eq.(5) to zero. Thus, the condition $\vec{q} = \vec{g}$ leads to the appearance of monochromatic radiation. This phenomenon has been considered to BS in details in Ref [19]. There is the same mechanism of constructive interference for PR. For CXR the equality $\vec{q} = \vec{g}$ makes small the denominator $\left(\vec{q}+\vec{k}\right)^2 - k^2$ in Eq.(6), but not equal to zero. This condition is similar to the known Bragg condition. Because of this CXR has the separate reflexes with angular dimensions of the order of γ^{-1} in the directions $\vec{v} - \omega^{-1}\vec{g}$. The reflexes for different $\vec{g}$ are partly covered at projectile energies of the order of several MeV. At this point CXR differs from coherent bremsstrahlung (CBS), so as CBS for all reciprocal lattice vectors is directed forward. This circumstance permits to select CXR from CBS by choosing the observation angle $\theta > \gamma^{-1}$.

Eqs.(5,6) are valid for those projectile energies at which the inequality $\gamma < \omega/\omega_p$ holds, ω_p is the plasma frequency of the crystal medium. If this relation breaks, then we have to replace ω in Eq.(6) by $\varepsilon_0^{1/2}\omega$, where ε_0 is a middle dielectric permittivity of the crystal. It leads to limitation of the CXR yield increase, as γ is unlimitly increased due to the density effect ([21]).

B. Method

The main task of the code is to calculate a number of coherent photons under CXR peaks, and a shape of a CXR line, as a function of the crystal target orientation with respect to the

particle beam direction. The CXR code calculates the number of coherent photons under the peaks by the following formula:

$$N_\gamma(\varphi,\theta) = \frac{t'}{V\Omega_0}\frac{1}{N_p}\sum_{j=1}^{N_p}\sum_{i=1}^{\Omega_0} d\sigma_i^j(\varphi_i,\theta_i)\,, \tag{7}$$

where t' is the thickness of the target along the beam axis; Ω_0 is the mean number of scattering events in the target; N_p is the number of the relativistic particles passing through the target; $d\sigma_i^j(\varphi_i,\theta_i)$ is the cross section of the radiation, generated by the projectile moving along the ith straight path of its track; φ_i is an angle between a set of crystallographic planes, on which the radiation is generated, and the ith segment of the track; θ_i is the observation angle for a photon emitted at this motion; angles φ,θ mean the same as φ_i,θ_i, but with respect to the beam axis (Fig. 2).

The shape of a CXR line at a given crystal orientation is obtained by calculating the distribution of $N_\gamma(\varphi,\theta)$ over ω.

C. Program organization

The computer code CXR has been written in Turbo Pascal, version 7.0. The list of the input parameters used and their allowed ranges are presented below.

Parameter name	Range allowed	Note
PLANE	(111)...(533)	Miller's indexes of those crystal planes on which the radiation is generated.
Z	6, 14, 32	Nuclear charge of the crystal atoms.
N_p	1..2500	Number of particles passing through the target during the MC calculation.
Channel, eV	1..20	Energy scale of a channel in that spectrum which presents shape of CXR line.
Detector FWHM, eV	1..5000	FWHM of the detector to be used in measurements.
Detector	0/1	Detector resolution will be (1) or will not be (0) taken into account.
Scattering	0/1	Multiple scattering will be (1) or will not be (0) taken into account.
Number of FI-points	50..500	Number of steps by φ to be used in calculating a number of coherent photons under a CXR peak.
$\theta, rad.$	$\gamma^{-1}..\pi/2$	Observation angle.
E, MeV	3.5..500	Energy of the projectile.
$\varphi_{\min}, rad.$	$\gamma^{-1}..\varphi_{\max}/2$	Initial value of φ.
$\varphi_{\max}, rad.$	$2\gamma^{-1}..\theta$	Final value of φ.
$L, cm.$	100..1000	Length of the photon channel.
$\chi_0, rad.$	$10^{-4}..10^{-2}$	Initial divergence of the particle beam.
e_0	1/-1/0	Charge of the projectile. If 0 is set it means that the static radiation component is "turned off".
t, cm	$10^{-3}..3 \times 10^{-2}$	Thickness of the target.
$r, cm.$	$0.1/5/0.05\gamma^{-1}$	Radius of the detector aperture. If r is more than $0.05\gamma^{-1}$, then, it is assumed that $r = 0.05\gamma^{-1}$.
θ_{orient}, deg	0..20	Angle at which the work planes were cut off with respect to the face surface of the target.
$\varphi_{Fix}, rad.$	$\gamma^{-1}..\theta$	Fixed orientation of the target in calculating a shape of the CXR line.

1. Unit SCAT

This unit calculates the components of a unit vector directed along a projectile's momentum in the laboratory coordinate system. In this system axis z is directed along the particle beam axis, and the xz-plane passes through the beam axis and the photon channel axis (Fig. 2).

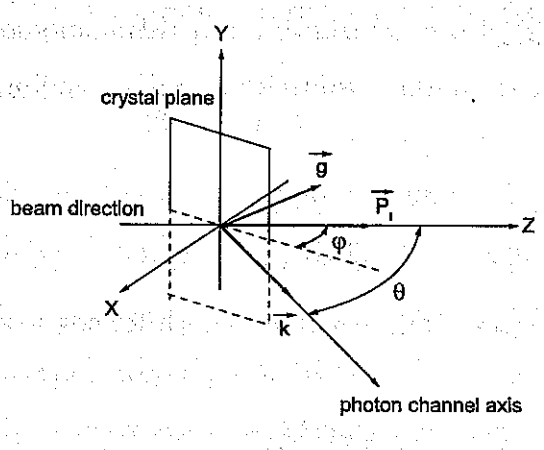

FIG. 2: The laboratory coordinate system and definitions used in the paper. $\overrightarrow{k}$ is the wave vector of a bremsstrahlung photon; the particle beam is directed along the z-axis and θ is the observation angle. The radiation is generated on a set of crystal planes, which are normal to the xz plane (scattering plane). Vector $\overrightarrow{g}$ lies in this plane and makes angle $\pi/2 - \varphi$ with the z-axis.

The particle track in the laboratory system is described by two angles: θ_e and φ_e. θ_e is the angle between the motion direction and the z-axis, and the angle φ_e is between the projection of the particle momentum on the xy-plane and the x-axis. Another coordinate system, the local system, where the particle moves along the z-axis, can be obtained from the laboratory system by rotation of an angle θ_e around the y-axis, and of an angle φ_e around the z-axis. The rotation matrix has the form:

$$A_{ij} = \begin{pmatrix} \cos\theta_e \cos\varphi_e & -\cos\theta_e \sin\varphi_e & \sin\theta_e \\ \sin\varphi_e & \cos\varphi_e & 0 \\ -\sin\theta_e \cos\varphi_e & \sin\theta_e \sin\varphi_e & \cos\theta_e \end{pmatrix}. \tag{8}$$

When the particle penetrates the target, an initial value of θ_e is generated in accordance with a Gaussian distribution using the algorithm of Ref. [22]:

$$\theta_e = \chi_0 \sqrt{-2 \ln \xi_1}, \tag{9}$$

and $\varphi_e = 2\pi\xi_2$. Throughout this paper we designate by ξ a random number uniformly distributed in the range [0,1]. The components of the unit vector along the projectile momentum are:

$$\widehat{p}_j = A_{zj}. \tag{10}$$

The initial coordinates of the local system origin are:

$$x_j^0 = 0, j = x, y, z. \tag{11}$$

According to Ref. [23] the mean number of scatterings occuring in a target of thickness t is

$$\Omega_0 = \left[\frac{94.0}{\beta}\right]^2 \frac{\rho t Z^{4/3}}{A}, \tag{12}$$

where ρ is the density of the scatterer, in g/cm^3, A is the atomic weight and t is in cm. The mean free path of the projectile in the target is

$$\Delta t = t/\Omega_0. \tag{13}$$

After passing the distance Δt the particle will be scattered and, in the local coordinate system, the angle θ_e is defined from the single-scattering probability:

$$\theta_e = \chi_B \sqrt{\frac{\xi_1}{1-\xi_1}}, \tag{14}$$

where χ_B is the Born screening angle ([23]):

$$\chi_B = \frac{1.13}{137} Z^{1/3} \gamma^{-1}. \tag{15}$$

The angle φ_e is defined as $2\pi\xi_2$. The coordinates of the local system origin are calculated by

$$x_j = x_j^0 + A_{zj}\Delta t, \tag{16}$$

and then we put $x_j^0 = x_j$. The angles θ_e and φ_e are calculated and then a rotation matrix A'_{ki}, which describes the connection between the old (before scattering) and the new (after scattering) local coordinate systems, is formed. The connection between the local coordinate system after scattering and the laboratory coordinate system is described by the matrix

$$B_{kj} = A'_{ij}A_{ki} \tag{17}$$

and then we equate the matrixes A and B. The current components of the unit vector along the particle momentum are defined by Eq.(10).

2. Unit PHOT

This unit calculates the components of the photon wave vector in the laboratory coordinate system. It is assumed that the photon collimator is circular. An entering photon point has coordinates:

$$x = r\xi_1\cos(2\pi\xi_2)\cos\theta + L\sin\theta; y = r\xi_1\sin(2\pi\xi_2); z = -r\xi_1\cos(2\pi\xi_2)\sin\theta + L\cos\theta. \tag{18}$$

It is supposed that in the local coordinate system the coordinates of a point, where a photon is radiated (PR), is $(0, 0, \Delta t/2)$ and, therefore, its coordinates in the laboratory system are

$$x'_j = x_j^0 + A_{zj}\Delta t/2, \tag{19}$$

where x_j^0 are defined by Eq.(16). Then, an unit vector directed along a photon wave vector has the components:

$$\widehat{k}_x = K^{-1}(x - x'_x); \widehat{k}_y = K^{-1}\left(y - x'_y\right); \widehat{k}_x = K^{-1}(z - x'_z), \tag{20}$$

where $K = \left((x - x'_x)^2 + \left(y - x'_y\right)^2 + (z - x'_z)^2\right)^{1/2}$.

3. Unit ATTEN

This unit calculates the attenuation of the photon flux in the target, on a path length from PR to a point where it leaves the target (PL), and in a detector window. The coordinates of PL are (t_x, t_y, t_z), where

$$t_x = \frac{t' - x'_z + \widehat{k}_z \widehat{k}_x^{-1} x'_x}{\widehat{k}_z \widehat{k}_x^{-1} + \tan\varphi}; t_y = x'_y + \widehat{k}_y \widehat{k}_x^{-1} \left(t_x - x'_x\right); t_z = t' - t_x \tan\varphi, \tag{21}$$

where $t' = t/\cos\varphi$. The path length which the photon passes in the target is

$$L_{abs} = \left(\sum_{j=x,y,z} \left(x'_j - t_j\right)^2 \right)^{1/2}. \tag{22}$$

We assume that the orientation of the crystalline target is such that the coherent scattering process of the radiated photons does not occur. Therefore, the attenuation factor has the form $\exp\left(-\mu_T(\omega) L_{abs} - \mu_W(\omega) L_W\right)$, where L_W is the detector window thickness; $\mu_T(\omega)$ and $\mu_W(\omega)$ are the attenuation coefficients at a given ω for the target and the detector window material, respectively. In the code we use the following representation for these functions:

$$\mu(\omega) = \rho \sum_i a_i \omega^i. \tag{23}$$

The values of a_i (Tables 1-4) for beryllium, diamond, silicon and germanium were calculated by using the data from Ref. [24].

4. Unit GLOBAL

This unit contains definitions of physical constants (lattice periods, densities, atomic weights, etc.) and a set of functions for calculation of the required physical values. The list of the functions is given below.

Name of the function	**Result, dimension**
CellVolume	returns the value of unit cell volume, cm^3
ReciprocalVector	returns the module of a reciprocal lattice vector, cm^{-1}
StructureFactor	returns the crystal structure factor, dimensionless
FormFactor	returns the atomic form factor for given Z and PLANE.
RotationMatrix	calculates the rotation matrix, Eq(8).
StartRotationMatrix	calculates the initial rotation matrix.
StartValues	calculates the values required for SCAT.
MaterialDefinition	definition of physical constants.
AbsoluteCoefficient	returns the coefficient in the cross section formula.
CrossSection	returns the value of the radiation cross section.

It is assumed that the radiation can be generated on the planes with the following Miller's indexes: (111), (220), (222), (311), (331), (420), (422), (511), (333), (440), (531), (442), (533). In calculating the form factor for (111) and (220) planes of silicon and diamond we use experimental known values, Ref. [25]. In all other cases we approximate the form factor function by the following expression ([26]):

$$F(g) = c + \sum_{i=1}^{4} a_i \exp\left(-b_i q^2\right), \tag{24}$$

where $q = g/4\pi$ and the coefficients a_i, b_i are presented in Table 5.

5. Unit CXRUI

This unit contains a set of procedures which provides the user interface. It gives a possibility to change parameters required for calculations, to visualize results of calculations, to save these results to the data file with a name defined by a user.

6. Unit CHANCE

It contains the function `RGenerator`, which is the random number generator. For more details see Ref. [27].

7. Unit NUMBER

This unit calculates the number of photons under a CXR peak as a function of φ by calling the SCAT, PHOT and ATTEN units. At each fixed φ the calculations are performed until the inequality $x_z^0 < t' - x_x^0 \tan\varphi$ is fulfilled, i.e. until the projectile is inside the target.

8. Unit LINE

This unit calculates the shape of a CXR line at a given φ_{Fix} by calculating a distribution of $N_\gamma(\varphi, \theta)$, Eq.(7), over ω. The distribution is presented by a spectrum $S(i)$, which has N_0 channels, $N_0 = 500$. The energy scale is defined by users. To take a finite value of detector resolution into account, the CXR code convolutes $S(i)$ with a function of detector response, which is assumed as a Gaussian one. The resulting spectrum, $S'(i)$, has the form:

$$S'(i) = \frac{1}{\sqrt{\pi}\sigma} \sum_{i_0=1}^{N_0} S(i_0) \exp\left(-\frac{(i-i_0)^2}{\sigma^2}\right), \tag{25}$$

where $\sigma = 0.6\text{FWHM}$, and a value for the detector FWHM is defined by the users.

9. Unit CXRHLP

This unit provides a short help for users. The definitions of the used parameters and their allowed ranges are presented.

10. Unit CXRCTR

This unit provides a control for the ranges of those parameters which are put by users.

11. Units PRINT1, PRINT2

These units write results of the calculations to the output data files in ASCII format. Unit PRINT1 writes a number of photons under a CXR peak as a function of the angle φ. Unit PRINT2 writes a number of photons under a CXR peak as a function of ω.

12. Unit CXR

This is the main program in the code. It provides fulfillment of the tasks in accordance with a user choice through the main program menu.

D. Input data files

The data required for the CXR code are saved in two files: INTGPAR.CPR and REALPAR.CPR. INTGPAR.CPR contains the following integer parameters: PLANE, Z, N_p, Channel, Detector FWHM, Detector, Scattering, Number of FI-points. REALPAR.CPR contains the real parameters: θ, E, $\varphi_{\min}$, $\varphi_{\max}$, L, χ_0, e_0, t, r, θ_{orient}, φ_{Fix}. After each running the used parameters are written into the same files. If, by some reasons, one or the both files are absent, the CXR code creates them with values of the parameters defined by default. These values are: PLANE = 111, $Z = 14$, $N_p = 20$, Channel = 1, Detector FWHM = 350, Detector = 1, Scattering = 0, Numbet of FI-points = 100, $\theta = 0.3$, $E = 25$, φ_{min}=0.1, $\varphi_{\max} = 0.18$, $L = 450$, $\chi_0 = 3 \times 10^{-4}$, $e_0 = 1$, $t = 3 \times 10^{-3}$, $r = 0.15$, $\theta_{orient} = 0$, $\varphi_{Fix} = \theta/2$. Note that the input data files are not in the text format and, therefore, can not be edit by users.

E. Output files

Output data are saved into files in the text format. File names are defined by users. To easily work with standard graphics software (for example, with Origin), output data files have extension DAT. Data files have a heading, which contains information about used parameters and results of calculations organized as a table.

F. Example of run type

INTGPAR.CPR

PLANE = 111, Z = 14, N_p = 500, Channel = 1, Detector FWHM = 350, Detector = 1, Scattering = 1, Numbet of FI-points = 50.

REALPAR.CPR

$\theta = 0.3$, $E = 25$, $\varphi_{\min} = 0.1$, $\varphi_{\max} = 0.18$, $L = 450$, $\chi_0 = 0.001$, $e_0 = 0$, $t = 0.003$, $r = 0.15$, $\theta_{orient} = 0$, $\varphi_{Fix} = \theta/2$.

Number.DAT

```
Crystal :                    Silicon
Crystal plane :              (111)
Crystal thickness :          3.00E-03 cm.
Energy of the beam :         2.50E+01 MeV
Scattering angle :           3.00E-01 rad.
Photon channel length :      4.50E+02 cm.
Detector radius :            1.50E-01 cm.
Initial beam divergence :    1.00E-03 rad.
Particle Charge :            0.00E+00
Number of particles :        500
Angle FI          Function
1.0016000000E-01 1.7489533883E-05
1.0176000000E-01 1.8711545800E-05
...                ...
```

Line.DAT

```
Crystal :                    Silicon
Crystal plane :              (111)
Crystal thickness :          3.00E-03 cm.
Energy of the beam :         2.50E+01 MeV
Scattering angle :           3.00E-01 rad.
Photon channel length :      4.50E+02 cm.
Detector radius :            1.50E-01 cm.
Initial beam divergence :    1.00E-03 rad.
Particle Charge :            0.00E+00
Number of particles :        500
Fixed FI :                   1.50E-01 rad.
```

```
Energy              Function1          Function2
1.2919389052E+01 2.6402584237E-09 2.6934993195E-08
1.2920389052E+01 0.0000000000E+00 2.7200659155E-08
...                 ...                ...
```

Here `Function1` and `Function2` denote the values which do not take (`Function1`) and take (`Function2`) energy resolution of the detector into account.

G. Some graphic results

Fig. 3 a,b,c represents the results of a calculation in comparison with our experimental data ([3],[11]). The photon detector used in the measurements was a 5-mm Si(Li) solid-state detector, enclosed by a 25-μm Be window and placed directly into a vacuum photon channel, oriented at $\theta = 0.3059$ rad with respect to the beam axis, $L = 450$ cm and $r = 0.15$ cm. In Fig. 3(a) the number of coherent photons as a function of the rotation angle φ, calculated for a germanium (PLANE = 220) and silicon (PLANE = 111) crystals, is shown. For germanium crystal: $t = 54$ μm, $E = 25.4$ MeV; for the silicon case: $t = 30$ μm, $E = 25$ MeV. In both cases N_p was equal to 500. Note that for the chosen N_p, the electron beam energies and target thicknesses under consideration, the number of radiation events at each φ was about 3×10^4 and 4×10^4 for the silicon and germanium cases, respectively.

Fig. 3(b) shows the number of coherent photons as a function of φ for a silicon crystal with the same calculation parameters shown above, except that $E = 15$ MeV.

In Fig. 3(c) we compare the measured and calculated shape of a line of the radiation generated in the germanium crystal at $E = 25.4$ MeV, $\varphi_{Fix} = 0.17$ rad and $N_p = 1000$. The dashed line represents the MC results, and the solid line shows the spectral density resulting from the convolution of the MC data with the energy resolution function of the detector. It was assumed that the energy resolution of the detector is 2.8% at 22.5 MeV.

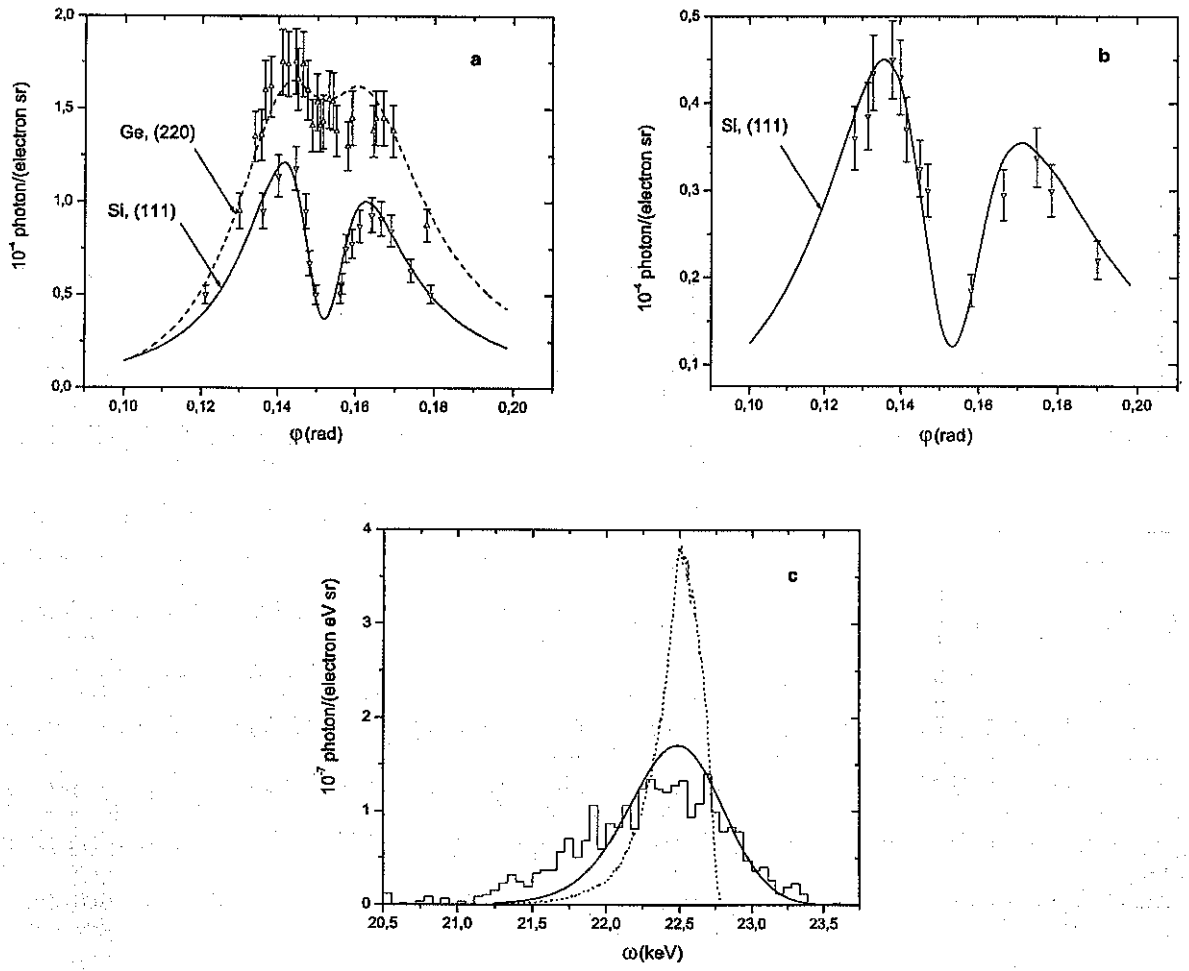

FIG. 3: (a) Calculated and observed angular dependence of number of CXR photons in germanium (E = 25.4 MeV) and silicon (E = 25 MeV) crystals; (b) The same as Fig.3a but for the silicon crystal at E = 15 MeV; (c) The observed and calculated spectral density of CXR for the germanium crystal (E = 25.4 MeV). The dashed line represents the MC result, and the solid line shows the spectral density resulting from the convolution of the MC data with the energy resolution function of the detector.

V. ACKNOWLEDGEMENTS

The authors wish to express their gratitude to FAPESP and CNq (Brazilian Agencies) for their partial support.

---

[1] S.A. Vorobev, B.N. Kalinin, S. Pak, A.P. Potylitsyn, JETP Letter., **41** (1985) 1.

[2] V.L. Morokhovskii, D.I. Adejishvili, V.B. Gavrikov, Ukrainian Phys. Jour., **38** (1993) 389.

[3] D.I. Adejishvili, V.B. Gavrikov, V.A. Romanov, Nucl. Instrum. Meth. Phys. Res. B **152** (1999) 406.

[4] D.I. Adejishvili, V.B. Gavrikov, *Coherent scattering of relativistic electron field in Ge on (220) planes*, in: Proc. of 24th Conf. on Physics of High-Energy Particle Interactions with Media, Moscow, 30 May - 1 June (1994) 58.

[5] J. Freudenberger, V.B. Gavrikov, M. Galemann, et al., Phys. Rev. Lett., **74** (1995) 2487.

[6] S.V.Blazhevich, G.L.Bochek, V.B.Gavrikov, et. al., Phys.Lett. A **195** (1994) 210.

[7] D.I.Adejishvily, V.B.Gavrikov, V.L.Morokhovskii, *About interference between parametric X-ray radiation of type B and coherent bremsstrahlung in a crystal*, Preprint KIPT 96-2 (1996) 9p.

[8] V.B. Gavrikov, V.P. Likhachev, V.A. Romanov, Nucl. Instrum. Meth. Phys. Res. A **457** (2001) 411.

[9] D.I.Adejishvily, V.B.Gavrikov, V.L.Morokhovskii *et al.*, *Line width of parametric X-radiation type B measured in germanium at electron energy 25.4 MeV*, Preprint KIPT 95-10 (1995) 5p.

[10] V.B. Gavrikov, Phd thesis, Kharkov Institute of Physics and Technology, 1996.

[11] V.B. Gavrikov, V.P. Likhachev, M.N. Martins, V.A. Romanov, Brazilian Journal of Physics, **29** (1999) 516.

[12] M.Ya. Amusia, Phys. Rep., 162, 5, 249 (1988).

[13] M.Ya. Amusia, M.Yu. Kuchiev, A.V. Korol', A.V. Solov 'ev, Sov. Phys. JETP **61** (1985) 224.

[14] V.N. Tsytovich, I.M. Oiringel (eds.), Polarization Bremsstrahlung , Plenum Publ., New York - London, 1992.

[15] V.B.Gavrikov, V.P.Likhachev, J.D.T. Arruda-Neto, and A.L. Bonini, Phys. Rev. A65(2001)022903

[16] V.B.Gavrikov, V.P.Likhachev, J.D.T. Arruda-Neto, and A.L. Bonini, Eur. Phys. J. A12(2001)487-493

[17] M.Ya. Amusia, V.M. Buimistrov, B.A. Zon, *et al.*, *Polarization Bremsstrahlung of Particles and Atoms*, Plenum Press, New York, 1992.

[18] H. Nitta, Phys. Rev. B **45** (1992) 7621.

[19] H. Uberall, Phys. Rev., **103** (1956) 1055.

[20] M.L. Ter-Mikaelian, *High-Energy Electromagnetic Processes in Condensed Media* (Wiley-Interscience) 1972.

[21] X. Artru, P. Rullhusen, Nucl. Instrum. Meth. Phys. Res. B **145** (1998) 1.

[22] W.H. Press, S.A. Teukolsky, W.A. Vetterling, B.P. Flannery, Numerical Recipes in FORTRAN, 2nd ed., Cambridge Univ. Press, Cambridge, 1992.

[23] W.T. Scott, Rev. Mod. Phys., **35** (1963) 231.

[24] B.L. Henke, E.M. Gullikson, J.C. Davis, Atomic Data and Nucl. Data Tabl., **54** (1993) 181.

[25] Von S. Gottlicher, E. Wolfel, Zeitschrift fur Elektrochemic, **63** (1959) 891.

[26] J. Wang, R.P. Sagar *et al.*, Atomic Data and Nucl. Data Tabl., **53** (1993) 233.

[27] B.A. Wichman, I.D. Hill, Apll. Statistics **31** (1982) 2, 18

Tables

Table 1. Coefficients in Eq.(23) for berilium.

	2.48 keV $\leq \omega <$ 5 keV	5 keV $\leq \omega <$ 15.5 keV	15.5 keV $\leq \omega <$ 31 keV
a_0	172.28	28.14	1.2
a_1	-71.11	-6.84	-0.067
a_2	7.6	0.56	0.001
a_3	-	-0.015	-

Table 2. Coefficients in Eq.(23) for diamond.

	$\omega <$ 5 keV	5 keV $\leq \omega <$ 15 keV	15 keV $\leq \omega <$ 33.4 keV
a_0	347.92	73.64	3.8
a_1	-126.86	-17.63	-0.35
a_2	12.23	1.446	0.012
a_3	-	-0.04	-0.00013

Table 3. Coefficients in Eq.(23) for silicon.

	$\omega < 4$ keV	4 keV $\leq \omega < 6.2$ keV	6.2 keV $\leq \omega < 15.5$ keV	15.5 keV $\leq \omega < 31$ keV
a_0	4064.85	3391.54	626.08	49.96
a_1	-1198.25	-1059.07	-137.08	-3.44
a_2	-9.54	85.83	10.37	0.06
a_3	20.54	-	-0.26	-

Table 4. Coefficients in Eq.(23) for germanium.

	12.4 keV $\leq \omega < 31$ keV
a_0	1144.88
a_1	-135.71
a_2	5.64
a_3	-0.078

Table 5. Coefficients for the presentation of the form factor function, Eq.(24).

	Diamond	Silicon	Germanium
a_1	2.31	6.2915	16.0816
a_2	1.02	3.0353	6.3747
a_3	1.5886	1.9892	3.7068
a_4	0.865	1.541	3.683
b_1	20.8439	2.4386	2.8509
b_2	10.2075	32.3337	0.2516
b_3	0.5687	0.6785	11.4468
b_4	31.6512	81.6937	54.7625
c	0.2156	1.1407	2.1313